Nano-Micro Lett. (2018) 10:60
https://doi.org/10.1007/s40820-018-0212-6

ARTICLE

Enhanced Performance of a Monolayer MoS_2/WSe_2 Heterojunction as a Photoelectrochemical Cathode

Jingwei Xiao[1] · Yu Zhang[1] · Huanjun Chen[1] · Ningsheng Xu[1] · Shaozhi Deng[1]

Received: 24 April 2018 / Accepted: 13 June 2018 / Published online: 3 July 2018

Highlights

- A vertical transition-metal dichalcogenide MoS_2/WSe_2 bilayer heterojunction was built by stacking a *P*-type WSe_2 and an *N*-type MoS_2 monolayer.
- An in situ measurement method was employed to characterize the intrinsic photoelectrochemical performance on the microscale.
- The photoelectrochemical current and the incident photo-to-current conversion efficiency of the MoS_2/WSe_2 bilayer heterojunction increased by a factor of 5.6 and enhanced 50% compared with the monolayer WSe_2 cathode.

Abstract Transition-metal dichalcogenide (TMD) semiconductors have attracted interest as photoelectrochemical (PEC) electrodes due to their novel band-gap structures, optoelectronic properties, and photocatalytic activities. However, the photo-harvesting efficiency still requires improvement. In this study, A TMD stacked heterojunction structure was adopted to further enhance the performance of the PEC cathode. A *P*-type WSe_2 and an *N*-type MoS_2 monolayer were stacked layer-by-layer to build a ultrathin vertical heterojunction using a micro-fabrication method. In situ measurement was employed to characterize the intrinsic PEC performance on a single-sheet heterostructure. Benefitting from its built-in electric field and type II band alignment, the MoS_2/WSe_2 bilayer heterojunction exhibited exceptional photocatalytic activity and a high incident photo-to-current conversion efficiency (IPCE). Comparing with the monolayer WSe_2 cathode, the PEC current and the IPCE of the bilayer heterojunction increased by a factor of 5.6 and enhanced 50%, respectively. The intriguing performance renders the MoS_2/WSe_2 heterojunction attractive for application in high-performance PEC water splitting.

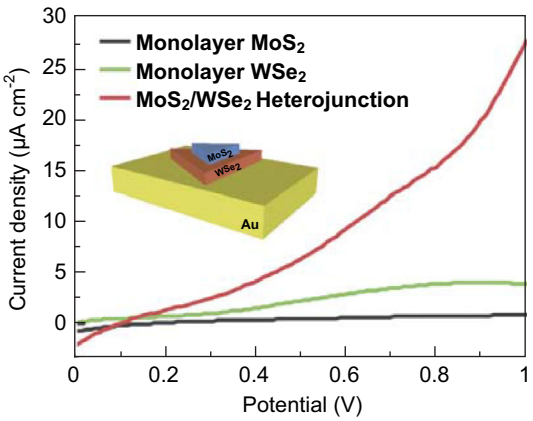

Keywords MoS_2/WSe_2 · Monolayer · Bilayer · Heterojunction · Photoelectrochemical cathode

✉ Yu Zhang
stszhyu@mail.sysu.edu.cn

[1] State Key Laboratory of Optoelectronic Materials and Technologies, Guangdong Province Key Laboratory of Display Material and Technology, School of Electronics and Information Technology, Sun Yat-sen University, Guangzhou 510275, People's Republic of China

1 Introduction

Hydrogen-based energy is a clean, sustainable, and highly efficient energy resource. Intensive research has been conducted to realize efficient production of hydrogen, and photoelectrochemical (PEC) water splitting is considered as a promising method [1–5]. A high-performance electrode material that can fully utilize solar energy and efficiently run water redox reactions is the key to PEC application. Recently, transition-metal dichalcogenide (TMD) semiconductors (MoS_2, WSe_2, WS_2, etc.) have been proposed as candidates for PEC electrode materials due to their novel band-gap structures, superior electrochemical properties and low cost [5, 6]. When the thickness of TMDs is varied from bulk to single layer, which become two-dimensional (2D) materials, their band gaps change from indirect (1.0–1.6 eV) to direct (1.6–1.8 eV) [7]. 2D material is a kind of layered material that consists of single or few atomic layers, such as graphene. The 2D material family contains carbon material, TMDs and layered metal oxides, etc. [8]. The change of band gaps allows 2D TMDs to absorb visible light, thus improving the photoconversion efficiency [9–11]. Additionally, layered TMDs have high absorption coefficients, permitting the absorption of 5–10% of incident sunlight by monolayer TMD [12]. All these features make layered TMDs attractive materials for solar-driven water-splitting devices.

In the group of TMDs, WSe_2 and MoS_2 are the choices with the best properties. *P*-type WSe_2 has been identified as an active and promising electrocatalyst for the hydrogen evolution reaction (HER) [13, 14]. Monolayer WSe_2 has a direct band gap of $\sim$ 1.65 eV, which corresponds to $\sim$ 750 nm wavelength light, and exhibits a high hole mobility ($\sim$ 140 $cm^2\ V^{-1}\ s^{-1}$) that is suitable for PEC cathodes [13, 15, 16]. Recent reports have demonstrated favorable PEC properties of WSe_2. A large-area WSe_2 flake Pt-decorating thin film fabricated using a space-confined self-assembled thin film deposition method demonstrated good PEC performance [14].

N-type MoS_2 has also been demonstrated to be an active catalyst in photocatalytic reactions [4, 17, 18]. Monolayer MoS_2 has a direct band gap of 1.85 eV and an electron mobility of 200 $cm^2\ V^{-1}\ s^{-1}$ [19]. Yu et al. reported its catalytic activity for hydrogen evolution [20], and Chen et al. and King et al. reported its application using silicon as a photocathode for PEC water splitting [21, 22].

Nevertheless, the PEC efficiency of few-layer or single-layer WSe_2 as a photocathode is still limited. To further improve the efficiency, coupling WSe_2 with a MoS_2 monolayer sheet to form a heterojunction could be an ideal choice. Owing to the suitable band gap and band position of the components, it has been reported that the MoS_2/WSe_2 heterojunction can be applied as a high-performance *p–n* diode [23] and transistor [24, 25]. As a PEC cathode, the advantages of the TMD heterojunction are that: (1) the built-in field in the depletion layer of the *p–n* junction may accelerate separation of the photo-generated excitons, as well as restrict recombination of the electron–hole pair to improve the PEC performance [26–28]; (2) the atom-thin vertical heterojunction could shorten the diffusion distance and rapidly deliver the excitons to the solid–liquid interface for redox reaction [17, 29]; (3) due to the large contact area in the heterojunction, more charge could be efficiently separated simultaneously; (4) an extended region of the visible-light spectrum could be utilized by this MoS_2/WSe_2 heterojunction.

In this study, we fabricated a 2D MoS_2/WSe_2 heterojunction PEC cathode and demonstrated its improved PEC performance. A micro-fabrication method is adopted to build a single-sheet stacked bilayer heterostructure. In situ measurement is employed to characterize the intrinsic PEC performance of the micro-heterostructure. The mechanism of enhancement of the PEC characteristics of the 2D heterojunction is also discussed.

2 Experimental

We fabricated a single-sheet MoS_2/WSe_2 heterojunction PEC device on the microscale and adopted an in situ measurement technique to characterize its performance. This is an advance method of characterizing the intrinsic PEC characteristics of heterojunction devices due to the unique material properties of a single sheet. Most of the interference factors such as the grain boundary, defects and inhomogeneity are eliminated in the single-sheet device by using in situ measurement.

2.1 Synthesis and Transfer of PEC Cathode Materials

Monolayer WSe_2 and MoS_2 were firstly synthesized on respective sapphire and SiO_2/Si substrate using chemical vapor deposition. The WSe_2 and MoS_2 sheets were then transferred to the PEC Au cathode on a silicon substrate to form the heterojunction. Specifically, polystyrene (PS) was first spin-coated onto the sapphire substrate and the substrate was then immersed in deionized water. The PS film with the WSe_2 sheet was peeled off from the substrate due to its hydrophobicity and then pasted on a bulk polydimethylsiloxane (PDMS). Using a microscope platform, the WSe_2 sheet on PDMS could be located and shifted to the top of the target Au electrode. WSe_2 with the PS layer was heated for exfoliation from PDMS and transferred to the Au electrode. Finally, the PS was removed using

methylbenzene, leaving the exfoliated WSe_2 sheet on the target electrode. The material characteristics were confirmed from the Raman and photoluminescence (PL) spectra (RENISHAW, 532 nm laser, 70 μW incident power) and atomic force microscopy (AFM) (NT-MDT NTEGRA Spectra). The light absorption spectra of monolayer MoS_2, WSe_2 and MoS_2/WSe_2 heterojunction were measured by HITACHI U-4100 spectrophotometer.

2.2 Fabrication of Devices

The single-sheet PEC device was fabricated using a microfabrication and transfer method. A 50 m wide Au thin film was sputtered onto a Si substrate with a 300 nm oxide layer, as the cathode. A WSe_2 flake was first transferred onto the Au electrode as the bottom layer of the heterojunction. The MoS_2 flake was transferred on top of the WSe_2 flake to form a vertical heterojunction (Fig. 1a). Another Au electrode on the other side of the substrate acted as the anode. The gap between the anode and cathode was 1.5 mm. Thereafter, the whole substrate was coated with photoresist, except for the area of the target heterojunction and the Au anode. This ensured that only the heterojunction and Au electrode were exposed to the solution and blocked the background noise. Two Al wires were, respectively, bonded onto the two Au electrode pads to output the PEC signal and connect the external measurement circuit (Fig. 1b).

2.3 PEC Measurement

An optical microscope (Olympus BX53) with a high-power mercury lamp (U-RFL-T, 100 W) was used as a PEC measurement platform. The device was steadily fixed on the sample stage of the microscope. The PEC measurement circuit of the device is shown in Fig. 1b. A Keithley 2600 Dual-Channel System Source Meter was used to apply a bias voltage and measure the current. The MoS_2/WSe_2 heterojunction connected to the negative pole of the power source acted as the cathode, while the Au anode was connected to the positive pole. A droplet of electrolyte (0.5 mol L^{-1} Na_2SO_4 solution) was injected to cover the whole device. During the measurement, white light from a mercury lamp, simulating solar power, was used to illuminate the device. The illuminated area was controlled to as small as 0.2 mm in diameter by the pinhole of the microscope. An external voltage was applied to the working electrode and swept from 0 to 1 V (100 mV s^{-1}), and the PEC current was recorded. To evaluate the relation of the PEC current to the visible-light spectrum, monochromatic light was separated from the white light using several optical filters (THORLABS, Optical bandwidth 10 nm). Optical filters were placed into the light path to select a specific wavelength. An optical power meter (GENTEC-EO UNO) was used to measure the incident light power of the different wavelengths, and a spot analyzer was used to confirm the size of the light spot.

3 Results and Discussion

3.1 Raman and PL Spectra of Monolayer Heterojunction

The optical image of the monolayer MoS_2/WSe_2 heterojunction is shown in Fig. 2a. A triangular MoS_2 sheet was stacked on a larger triangular WSe_2. These two stacked monolayer sheets formed a vertical heterojunction. The AFM showed that the step heights of monolayer WSe_2 on the Au electrode and that of monolayer MoS_2 on WSe_2 were 0.7 and 0.8 nm, respectively, which confirmed the monolayer thickness of the WSe_2 and MoS_2 sheet (Fig. 2b).

The Raman and PL spectra of the mono-MoS_2, WSe_2, and MoS_2/WSe_2 heterojunction were acquired to characterize their crystallinity. Figure 2e shows the Raman

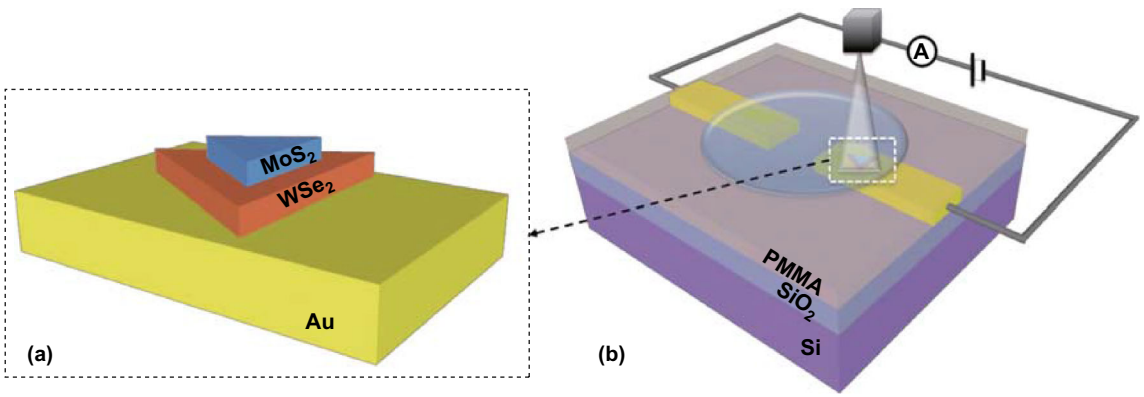

Fig. 1 Schematic of **a** the MoS_2/WSe_2 heterojunction and **b** PEC device and measurement

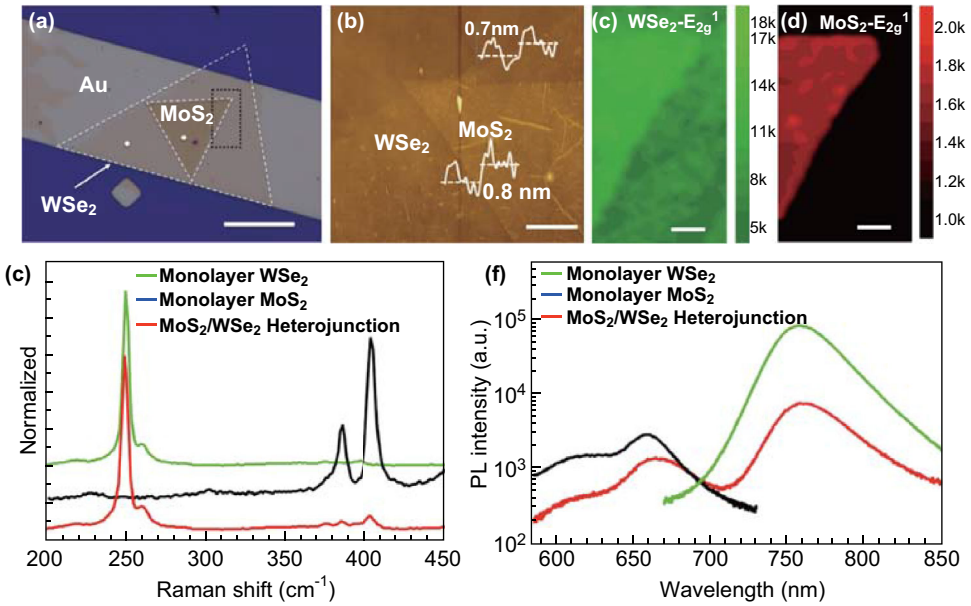

Fig. 2 **a** Optical image of monolayer MoS_2/WSe_2 heterojunction (dashed in white triangle). The white dots marked in the optical image are the spots where the spectra are accumulated (scale bar is 30 m). **b** AFM scanning showing thickness of surface of MoS_2/WSe_2 heterojunction and line scan profile (scale bar is 4 m). **c**, **d** Raman intensity map of the WSe_2 E^1_{2g} mode (green) and MoS_2 E^1_{2g} mode (red) in heterostructure, corresponding to black dashed square area in (**a**) (scale bar is 5 m). **e**, **f** Raman and PL spectra of monolayer MoS_2 (black line), WSe_2 (green line) and MoS_2/WSe_2 heterojunction (red line). (Color figure online)

spectra of the above three materials. Monolayer WSe_2 has showed two strong peaks around 250 cm^{-1} corresponding to the E^1_{2g} (in-plane) and A_{1g} (out-of-plane) modes. The Raman B^1_{2g} mode at 310 cm^{-1} was not observed, which confirmed the monolayer sheet structure [30–32]. Monolayer MoS_2 showed characteristic E^1_{2g} and A_{1g} Raman mode signals at 385.0 and 405.6 cm^{-1}, consistent with published reports [33–35] (Fig. 2e, black line). The Raman spectrum of the MoS_2/WSe_2 heterojunction showed all the peaks of single-layer WSe_2 and MoS_2. The peak intensity of WSe_2 was much stronger than MoS_2 [35]; therefore the Raman peak intensity of MoS_2 obtained in heterojunction looks weaker. Actually, the Raman peak intensity of MoS_2 in the heterojunction is the same as that of single-layer MoS_2. The Raman mapping is used to further verify the crystal homogeneity of MoS_2 and WSe_2 in their heterostructure, as shown in Fig. 2c, d. The Raman intensity mapping used the E^1_{2g} mode of both WSe_2 and MoS_2, which the color scale bar represents the intensity, respectively. In the overlapping area, the Raman intensity of WSe_2 was stronger. The reason is related to the heterojunction stacking that active the Raman features.

The PL spectrum for monolayer WSe_2 in Fig. 2f shows a strong single PL peak around 760 nm, nearly 1.63 eV, corresponding to the "A" exciton peak (Fig. 2e, green line). The strong emission and single symmetric PL peak at $\sim$ 1.60 eV suggest the direct band-gap nature of monolayer WSe_2 [33, 35, 36]. It is reported that the PL spectrum of multilayer WSe_2 shows the "A" exciton peak and an additional broad peak at $\sim$ 885 nm (call as "I" peak), which is attributed to indirect band-gap emission [36, 37]. Single-layer MoS_2 showed a peak at 670 nm, nearly 1.85 eV, corresponding to "A" exciton. The PL yield of WSe_2 was much higher than that of MoS_2, suggesting stronger nonradiative recombination in the latter. The PL peak of WSe_2 in heterostructure was about ten times lower than that of the individual WSe_2. Such a significant quenching effect indicated that many photo-generated charge carriers were transferred from WSe_2 to MoS_2 [25, 33, 35, 36].

3.2 PEC Performance of Bilayer Heterojunction

The PEC current of single-layer WSe_2, MoS_2 and the heterojunction immersed in 0.5 mol L^{-1} Na_2SO_4 solution was measured under illumination with white light in order to investigate their PEC performance. The PEC current–voltage (*J*–*V*) curves of the above three materials under illumination are shown in Fig. 3a. MoS_2 presented nearly no current response (Fig. 3a, black curve) owing to its intrinsic *n*-type characteristic. The Fermi level of the *n*-type semiconductor is higher than the electrochemical potential; hence, electrons will transfer from the semiconductor to the solution until the equilibration is achieved. After that, the bands of *n*-type semiconductor bend upward, which forms a barrier on the solid–liquid interface and

blocks the transport of electrons [5]. This barrier layer hinders its catalytic activity as a PEC cathode. WSe_2 presented a better PEC current response to the white light. A current density of 5 A cm^{-2} was recorded when the potential was swept to 1 V (Fig. 3a, green curve). As a *p*-type semiconductor, WSe_2 [30, 38] is suitable for use as a PEC cathode. Due to its lower Fermi level, the bands of the *p*-type semiconductor bend downward when it is contacted with electrolyte solution. Without the barrier at the solid–liquid interface, the photo-generated electrons in WSe_2 are easier to be driven toward the interface and move into the solution [5]. This bending facilitates the photo-generated electrons to reduce H^+ and to transport more efficiently. The PEC current of the WSe_2/MoS_2 heterojunction (Fig. 3a, red curve) showed a much larger increase than the two aforementioned samples. A PEC current density of up to 28 μA cm^{-2} at 1 V bias was observed with the heterojunction, which is 5.6 times as large as that of WSe_2. This provides initial evidence of the positive effect of the heterojunction on the PEC reaction.

The PEC current response curve was constructed for comparison with the visible-light response of the three aforementioned samples (Fig. 3b). The applied voltage was 1 V. All three samples exhibited a fast-optical response when the light was switched between the on and off states. In the light-on state, the decay of the PEC current is caused by the recombination of photo-generated electrons and holes. When illumination was interrupted, the photo-generated electrons at the surface suddenly vanished, and a gradually decline of the current was observed. Under the same illumination and bias conditions, the PEC current density of the MoS_2/WSe_2 heterojunction was three times as large as that of WSe_2. This result is consistent with a former report that the heterojunction performed better than the single-material congeners in the PEC reaction [36, 39, 40].

3.3 IPCE of Different Nanosheets

The incident photon-to-current conversion efficiency (IPCE) was measured and calculated for quantitative comparison of the light harvesting efficiency of the WSe_2 and MoS_2/WSe_2 heterojunctions as a function of the wavelength. The IPCE (η) is defined as the ratio of the incident monochromatic photons converted to collected electrons and can be calculated by using Eq. 1

$$\eta = \frac{I_{ph}}{P} \times \frac{1240}{\lambda} \times 100\% \quad (1)$$

here I_{ph} (A) is the photocurrent, P (W) is the incident light power, and λ (nm) is the wavelength of light. The IPCE varied with different incident wavelength (λ). As shown in

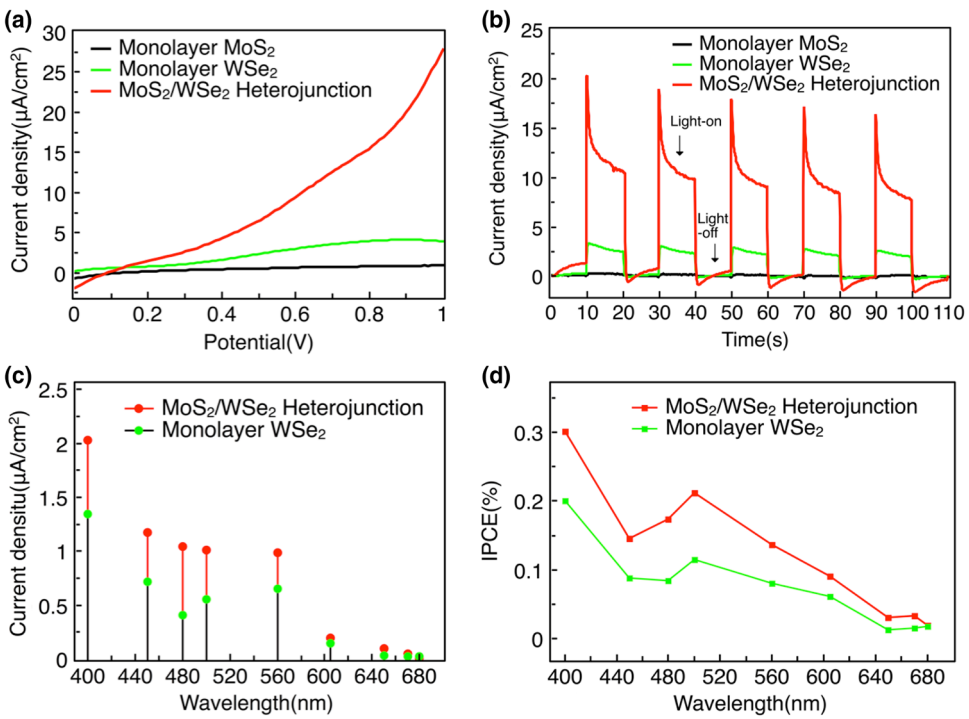

Fig. 3 **a** PEC current density versus voltage (*J*–*V*) curves of MoS_2/WSe_2 heterojunction (red), monolayer WSe_2 (green), and monolayer MoS_2 (black) under the same white light illumination conditions. **b** Current response curves for the three samples under 1 V external bias with illumination an interval of 10 s. **c** PEC currents of monolayer MoS_2/WSe_2 heterojunction (red dots) and WSe_2 (green dots) at different wavelengths. **d** IPCE of MoS_2/WSe_2 heterojunction (red dots line) and WSe_2 (green dots line). (Color figure online)

Fig. 3c, the PEC current density of the heterojunction and WSe_2 was measured at wavelengths from 400 to 680 nm wavelength at bias of 1 V. The achieved PEC current density was smaller under monochromatic light than that obtained under white light given that the intensity of the monochromatic light decreased when filtered from the white light.

It was found that the heterojunction had a higher (Fig. 3c, red dots) current density in comparison with WSe_2 (Fig. 3c, green dots) at all wavelengths. For example, the current density of the heterojunction at 480–500 nm was nearly twice as large as that of WSe_2. The corresponding IPCEs of the heterojunction (red dot line) and WSe_2 (green dot line) were calculated, as shown in Fig. 3d. Compared to the WSe_2 counterpart, the MoS_2/WSe_2 heterojunction showed an obvious enhancement of the IPCE in the range of 400–680 nm. At 400 nm, the IPCE of the heterojunction exhibited a maximum value of 0.3%, which is 50% higher than that of WSe_2. This is attributed to the highest absorption peak of WSe_2 around 420 nm [29, 41], and the absorption rate in 400 nm is close to that in 420 nm. In addition, the WSe_2/MoS_2 heterojunction helps to increase the electron–hole separation efficiency. Therefore, the IPCE was largely improved with the heterojunction. The IPCE of the heterojunction was around 0.1–0.3% at 450–605 nm and decreased with a red-shift of the wavelength due to the reduced absorption of light at higher wavelength.

The light absorption spectra of monolayer MoS_2, WSe_2 and MoS_2/WSe_2 heterojunction are shown in Fig. 4, which is consistent with former reports [29, 41–43]. The absorption spectrum of monolayer WSe_2 (Fig. 4, green curve) possesses 3 peaks at ~ 420, 500, and 600 nm (labeled as D, C, B peak, respectively) in 400–700 nm. The

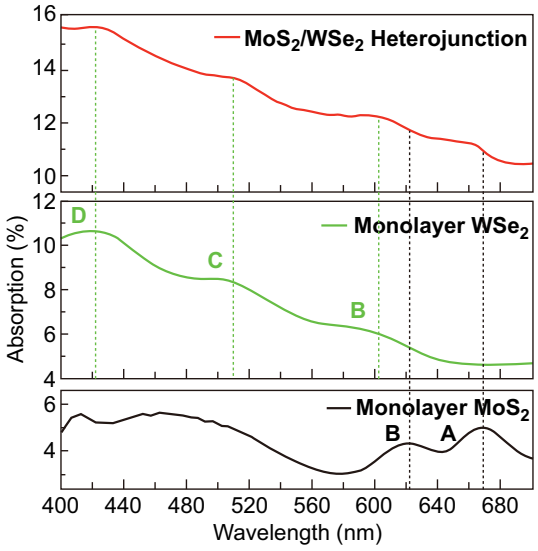

Fig. 4 Absorption spectra of MoS_2/WSe_2 heterojunction (red curve), monolayer WSe_2 (green curve) and monolayer MoS_2 (black curve). (Color figure online)

light absorptivity is between 4.5 and 11% and decreases with wavelength. There are two absorption peaks in the absorption spectrum of monolayer MoS_2 (Fig. 4, black curve) at ~ 620 and 670 nm (labeled as B and A peak, respectively). The light absorptivity is between 3.5 and 6%. The absorption spectrum of heterojunction (Fig. 4, red curve) is the sum of absorption spectrum of WSe_2 and MoS_2. The overall absorptivity is 1.5 times that of monolayer WSe_2. Because the heterojunction consists of WSe_2 and MoS_2, it exhibits the absorption characteristics of monolayer WSe_2 and MoS_2. The peak surrounding at 500 nm in both IPCE of WSe_2 and heterojunction is mainly due to the C absorption peak of monolayer WSe_2, where more light was utilized. It is remarkable that the IPCE analysis of the heterojunction showed a small peak at 670 nm, compared to that of WSe_2. This peak is attributed to the absorption of MoS_2 at ~ 670 nm [42, 43]. Thus, the MoS_2/WSe_2 heterojunction was able to harvest more photons under 670 nm irradiation than WSe_2. Meanwhile, the optical absorption of heterojunction can be improved by some means. For example, using nano-metal stripe to introduce surface plasmon resonances [44] or inserting a certain thickness of transparent electrode between heterojunction and back electrode to construct resonance back reflection [45] can further enhance light absorption.

Although monolayer WSe_2 has three absorption peaks at 400–700 nm and its absorption gradually decreases from 400 to 700 nm, the peak at 600 nm is relatively weak. MoS_2 has an enhanced absorption at ~ 670 nm. Therefore, the IPCE of the heterojunction was the highest at 400 nm and under excitation at the wavelengths of the two other peaks at 500 and 670 nm in the wavelength range of 400–680 nm. Overall, the improvement in the IPCE was mainly attributed to: (1) the *p*–*n* junction formed between MoS_2 and WSe_2, which increases the separation of the electron–hole pair; (2) broadening of the range of the solar spectrum absorbed by the stack of MoS_2 and WSe_2, leading to better utilization of the solar spectrum.

The energy band position of monolayer MoS_2 and WSe_2 compared with redox potentials of water splitting has shown in Fig. 5a. The relative band position between monolayer MoS_2 and WSe_2 is decided by their electron affinity. The electron affinity of WSe_2 and MoS_2 is χ_{W-} ~ 3.7 eV and χ_M ~ 4.2 eV [46–48], respectively. For the heterojunction, the developed band alignment and built-in potential between *p*-WSe_2 and *n*-MoS_2 help to facilitate separation of the photo-generated exciton, as shown in Fig. 5b. Because MoS_2 and WSe_2 form a type II band alignment, the conduction band minimum (CBM) and valence band minimum (VBM) of WSe_2 are higher than those of MoS_2 [35, 36]. Upon irradiation, photons are absorbed and excitons are generated in single-layer WSe_2 and MoS_2. The photo-generated free electrons in the CBM

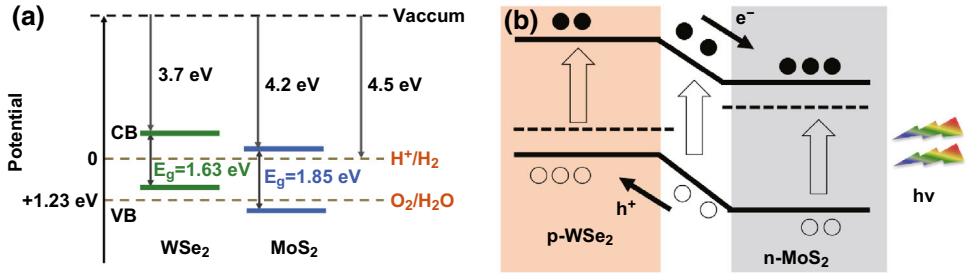

Fig. 5 **a** Energy band position of monolayer MoS_2 and WSe_2 compared with redox potentials for water splitting. **b** MoS_2/WSe_2 heterojunction formed a type II band alignment. When illuminated, photo-generated electrons are transferred from valence band to conduction band and the built-in electric field helps to separate excitons

of WSe_2 can be transferred to the CBM of MoS_2 owing to the large band offset between WSe_2 and MoS_2 [35, 36, 42]. Due to the built-in field existing across the stacking facet of WSe_2 and MoS_2, the photo-induced excitons then relax at the MoS_2/WSe_2 interface, driving more efficient separation [49]. The electrons then drift to the CBM of MoS_2 while the holes drift to the VBM of WSe_2. Hence, electrons are collected in the conduction band and transported to the solid–liquid interface. At the interface, the reduction reaction occurs at the surface of MoS_2, in which H^+ obtains electron to generate H_2 ($2H^+ + 2e^- \rightarrow H_2$). It is noted that due to the atomic thickness of the ultrathin heterojunction, its built-in field would penetrate to the solid–liquid interface, thus having a positive potential to overcome the barrier on the interface and accelerate the redox reaction. In addition, the ultrathin heterojunction shortens the path for electron transport. The electrons could reach the interface immediately after separation. Therefore, compared with the single-layer material, the heterojunction leads to better utilization of light and furnishes more electrons for the reaction. As a result, a much higher PEC current and a greater IPCE were achieved with the MoS_2/WSe_2 heterojunction in comparison with WSe_2 and MoS_2.

4 Conclusion

Monolayer *p*-type WSe_2 and monolayer *n*-type MoS_2 were stacked layer-by-layer to form a heterojunction by using a dry-transfer method. A WSe_2/MoS_2 heterojunction was fabricated to act as a miniaturized PEC cathode on the micrometer scale. In situ measurement was adopted to investigate the intrinsic PEC characteristics for comparison with the single-material cathode. The PEC current of the heterojunction was 5.6 times than that of the monolayer WSe_2 under an external bias of 1 V under illumination with white light. The bilayer heterojunction also exhibited a 50% enhancement in the IPCE relative to the monolayer WSe_2 within the visible light range of 400–680 nm. Derived from the type II band alignment formed between MoS_2, WSe_2 and the ultrathin thickness of the heterojunction, the heterojunction broadened the light harvesting range, improved the photo-induced exciton separation, and accelerated the carrier transport. The unique structure and superior PEC characteristics of the MoS_2/WSe_2 heterojunction suggest that it holds great promise as a photocathode for the HER with potential for efficient solar energy conversion applications.

Acknowledgements This work was supported by the National Natural Science Foundation of China (Grant Nos. 51290271, 51672314), the Guangdong Natural Science Foundation (Grant No. 2016A030313359), the Science and Technology Program of Guangzhou (Grant No. 201707010224), the Science and Technology Department of Guangdong Province, the Fundamental Research Funds for the Central Universities.

References

1. T. Hisatomi, J. Kubota, K. Domen, Recent advances in semiconductors for photocatalytic and photoelectrochemical water splitting. Chem. Soc. Rev. **43**(22), 7520–7535 (2014). https://doi.org/10.1039/C3CS60378D
2. J. Li, N. Wu, Semiconductor-based photocatalysts and photoelectrochemical cells for solar fuel generation: a review. Catal. Sci. Technol. **5**(3), 1360–1384 (2015). https://doi.org/10.1039/C4CY00974F
3. X. Chia, A. Adriano, Z. Sofer, J. Luxa, M. Pumera, Catalytic and charge transfer properties of transition metal dichalcogenides arising from electrochemical pretreatment. ACS Nano **9**(5), 5164–5179 (2015). https://doi.org/10.1021/acsnano.5b00501
4. X. Chen, Z. Zhang, L. Chi, A.K. Nair, W. Shangguan, Z. Jiang, Recent advances in visible-light-driven photoelectrochemical water splitting: catalyst nanostructures and reaction systems. Nano-Micro Lett. **8**, 1 (2016). https://doi.org/10.1007/s40820-015-0063-3

5. M.G. Walter, E.L. Warren, J.R. McKone, S.W. Boettcher, Q. Mi, E.A. Santori, N.S. Lewis, Solar water splitting cells. Chem. Rev. **110**(11), 6446–6473 (2010). https://doi.org/10.1021/cr1002326
6. A. Kudo, Y. Miseki, Heterogeneous photocatalyst materials for water splitting. Chem. Soc. Rev. **38**(1), 253–278 (2009). https://doi.org/10.1039/b800489g
7. X. Duan, C. Wang, A. Pan, R. Yu, X. Duan, Two-dimensional transition metal dichalcogenides as atomically thin semiconductors: opportunities and challenges. Chem. Soc. Rev. **44**(24), 8859–8876 (2015). https://doi.org/10.1039/c5cs00507h
8. A. Gupta, T. Sakthivel, S. Seal, Recent development in 2D materials beyond graphene. Prog. Mater. Sci. **73**, 44–126 (2015). https://doi.org/10.1016/j.pmatsci.2015.02.002
9. Q.H. Wang, K. Kalantar-Zadeh, A. Kis, J.N. Coleman, M.S. Strano, Electronics and optoelectronics of two-dimensional transition metal dichalcogenides. Nat. Nanotechnol. **7**(11), 699–712 (2012). https://doi.org/10.1038/nnano.2012.193
10. D. Jariwala, V.K. Sangwan, L.J. Lauhon, T.J. Marks, M.C. Hersam, Emerging device applications for semiconducting two-dimensional transition metal dichalcogenides. ACS Nano **8**(2), 1102–1120 (2014). https://doi.org/10.1021/nn500064s
11. R. Lv, J.A. Robinson, R.E. Schaak, D. Sun, Y. Sun, Y. Sun, T.E. Mallouk, M. Terrones, Transition metal dichalcogenides and beyond: synthesis, properties, and applications of single- and few-layer nanosheets. Acc. Chem. Res. **48**(1), 56–64 (2015). https://doi.org/10.1021/ar5002846
12. M. Bernardi, M. Palummo, J.C. Grossman, Extraordinary sunlight absorption and one nanometer thick photovoltaics using two-dimensional monolayer materials. Nano Lett. **13**(8), 3664–3670 (2013). https://doi.org/10.1021/nl401544y
13. F.R.F. Fan, H.S. White, B.L. Wheeler, A.J. Bard, Semiconductor electrodes. 31. photoelectrochemistry and photovoltaic systems with *n*- and *p*-type WSe_2 in aqueous solution. J. Am. Chem. Soc. **102**(16), 5142–5148 (1980). https://doi.org/10.1021/ja00536a002
14. X. Yu, M.S. Prévot, N. Guijarro, K. Sivula, Self-assembled 2D WSe_2 thin films for photoelectrochemical hydrogen production. Nat. Commun. **6**, 7596 (2015). https://doi.org/10.1038/ncomms8596
15. H. Zhou, C. Wang, J.C. Shaw, R. Cheng, Y. Chen et al., Large area growth and electrical properties of *p*-type WSe_2 atomic layers. Nano Lett. **15**(1), 709–713 (2015). https://doi.org/10.1021/nl504256y
16. H.J. Chuang, X. Tan, N.J. Ghimire, M.M. Perera, B. Chamlagain et al., High mobility WSe_2 *p*- and *n*-type field-effect transistors contacted by highly doped graphene for low-resistance contacts. Nano Lett. **14**, 3594–3611 (2014). https://doi.org/10.1021/nl501275p
17. J. Li, E. Liu, Y. Ma, X. Hu, J. Wan, L. Sun, J. Fan, Synthesis of MoS_2/g–C_3N_4, nanosheets as 2D heterojunction photocatalysts with enhanced visible light activity. Appl. Surf. Sci. **364**, 694–702 (2016). https://doi.org/10.1016/j.apsusc.2015.12.236
18. Z. Yin, B. Chen, M. Bosman, X. Cao, J. Chen, B. Zheng, H. Zhang, Water splitting: Au nanoparticle modified MoS_2 nanosheet based photoelectrochemical cells for water splitting. Small **10**(17), 3537–3543 (2014). https://doi.org/10.1002/smll.201400124
19. B. Radisavljevic, A. Radenovic, J. Brivio, V. Giacometti, A. Kis, Single-layer MoS_2 transistors. Nat. Nanotechnol. **6**(3), 147–150 (2011). https://doi.org/10.1021/nn2024557
20. Y. Yu, S.Y. Huang, Y. Li, S.N. Steinmann, W. Yang, L. Cao, Layer-dependent electrocatalysis of MoS_2 for hydrogen evolution. Nano Lett. **14**(2), 553–558 (2014). https://doi.org/10.1021/nl403620g
21. Y. Chen, P.D. Tran, P. Boix, Y. Ren, S.Y. Chiam, Z. Li, K. Fu, L.H. Wong, J. Barber, Silicon decorated with amorphous cobalt molybdenum sulfide catalyst as an efficient photocathode for solar hydrogen generation. ACS Nano **9**(4), 3829–3836 (2015). https://doi.org/10.1021/nn506819m
22. L.A. King, T.R. Hellstern, J. Park, R. Sinclair, T.F. Jaramillo, Highly stable molybdenum disulfide protected silicon photocathodes for photoelectrochemical water splitting. ACS Appl. Mater. Interfaces **9**(42), 36792–36798 (2017). https://doi.org/10.1021/acsami.7b10749
23. T. Roy, M. Tosun, X. Cao, H. Fang, D.H. Lien et al., Dual-gated MoS_2/WSe_2 van der waals tunnel diodes and transistors. ACS Nano **9**(2), 2071–2079 (2015). https://doi.org/10.1021/nn507278b
24. A. Nourbakhsh, A. Zubair, M.S. Dresselhaus, T. Palacios, Transport properties of a MoS_2/WSe_2 heterojunction transistor and its potential for application. Nano Lett. **16**(2), 1359–1366 (2016). https://doi.org/10.1021/acs.nanolett.5b04791
25. H. Fang, C. Battaglia, C. Carraro, S. Nemsak, B. Ozdol et al., Strong interlayer coupling in van der waals heterostructures built from single-layer chalcogenides. Proc. Natl. Acad. Sci. USA **111**(17), 6198–6202 (2014). https://doi.org/10.1073/pnas.1405435111
26. K. Zhang, T. Zhang, G. Cheng, T. Li, S. Wang et al., Interlayer transition and infrared photodetection in atomically thin type-ii $MoTe_2$/MoS_2 van der waals heterostructures. ACS Nano **10**(3), 3852–3858 (2016). https://doi.org/10.1021/acsnano.6b00980
27. A.K. Geim, I.V. Grigorieva, Van der waals heterostructures. Nature **499**(7459), 419–425 (2013). https://doi.org/10.1038/nature12385
28. C.H. Lee, G.H. Lee, A.M.V.D. Zande, W. Chen, Y. Li et al., Atomically thin *p–n* junctions with van der waals heterointerfaces. Nat. Nanotechnol. **9**(9), 676–681 (2014). https://doi.org/10.1038/NNANO.2014.150
29. K. Wang, B. Huang, M. Tian, F. Ceballos, M.W. Lin et al., Interlayer coupling in twisted WSe_2/WS_2 bilayer heterostructures revealed by optical spectroscopy. ACS Nano **10**(7), 6612–6622 (2016). https://doi.org/10.1021/acsnano.6b01486
30. J.K. Huang, J. Pu, C.L. Hsu, M.H. Chiu, Z.Y. Juang et al., Large-area synthesis of highly crystalline WSe_2 monolayers and device applications. ACS Nano **8**(1), 923–930 (2013). https://doi.org/10.1021/nn405719x
31. E. Del Corro, H. Terrones, A. Elias, C. Fantini, S. Feng, M.A. Nguyen, T.E. Mallouk, M. Terrones, M.A. Pimenta, Excited excitonic states in 1L, 2L, 3L, and bulk WSe_2 observed by resonant Raman spectroscopy. ACS Nano **8**(9), 9629–9635 (2014). https://doi.org/10.1021/nn504088g
32. B. Liu, M. Fathi, L. Chen, A. Abbas, Y. Ma, C. Zhou, Chemical vapor deposition growth of monolayer WSe_2 with tunable device characteristics and growth mechanism study. ACS Nano **9**, 6119–6127 (2015). https://doi.org/10.1021/acsnano.5b01301
33. P. Tonndorf, R. Schmidt, P. Bottger, X. Zhang, J. Borner et al., Photoluminescence emission and raman response of MoS_2, $MoSe_2$, and WSe_2 nanolayers. Opt. Express **21**(4), 4908–4916 (2013). https://doi.org/10.1364/OE.21.004908
34. H. Li, J. Wu, Z. Yin, H. Zhang, Preparation and applications of mechanically exfoliated single-layer and multilayer MoS_2 and WSe_2 nanosheets. Acc. Chem. Res. **47**(4), 1067–1075 (2014). https://doi.org/10.1021/ar4002312
35. B. Peng, G. Yu, X. Liu, B. Liu, X. Liang, L. Bi, L. Deng, T.C. Sum, K.P. Loh, Ultrafast charge transfer in MoS_2/WSe_2 *p–n* heterojunction. 2D Mater. **3**(2), 025020 (2016). https://doi.org/10.1088/2053-1583/3/2/025020
36. R. Cheng, D. Li, H. Zhou, C. Wang, A. Yin et al., Electroluminescence and photocurrent generation from atomically sharp WSe_2/MoS_2 heterojunction *p–n* diodes. Nano Lett. **14**(10), 5590–5597 (2014). https://doi.org/10.1021/nl502075n
37. W.J. Zhao, Z. Ghorannevis, L.Q. Chu, M.L. Toh, C. Kloc et al., Evolution of electronic structure in atomically thin sheets of WS_2

and WSe_2. ACS Nano **7**(1), 791–797 (2013). https://doi.org/10.1021/nn305275h
38. N. Flöry, A. Jain, P. Bharadwaj, M. Parzefall, T. Taniguchi et al., A $WSe_2/MoSe_2$ heterostructure photovoltaic device. Appl. Phys. Lett. **107**(12), 4785–4791 (2015). https://doi.org/10.1063/1.4931621
39. Y. Liu, Y.X. Yu, W.D. Zhang, MoS_2/CdS heterojunction with high photoelectrochemical activity for H_2 evolution under visible light: the role of MoS_2. J. Phys. Chem. C **117**(25), 12949–12957 (2013). https://doi.org/10.1021/jp4009652
40. Z. Huang, W. Han, H. Tang, L. Ren, D.S. Chander, X. Qi, H. Zhang, Photoelectrochemical-type sunlight photodetector based on MoS_2/graphene heterostructure. 2D Mater. **2**(3), 035011 (2015). https://doi.org/10.1088/2053-1583/2/3/035011
41. M.H. Chiu, M.Y. Li, W. Zhang, W.T. Hsu, W.H. Chang, M. Terrones, H. Terrones, L.-J. Li, Spectroscopic signatures for interlayer coupling in MoS_2–WSe_2 van der waals stacking. ACS Nano **8**(9), 9649–9656 (2014). https://doi.org/10.1021/nn504229z
42. Y. Zhang, M.M. Ugeda, C. Jin, S.F. Shi, A.J. Bradley et al., Electronic structure, surface doping and optical response in epitaxial WSe_2 thin films. Nano Lett. **16**(4), 2485–2491 (2016). https://doi.org/10.1021/acs.nanolett.6b00059
43. Y. Yu, S. Hu, L. Su, L. Huang, Y. Liu et al., Equally efficient interlayer exciton relaxation and improved absorption in epitaxial and non-epitaxial MoS_2/WS_2 heterostructures. Nano Lett. **15**(1), 486–491 (2015). https://doi.org/10.1021/nl5038177
44. L. Ju, B.S. Geng, J. Horng, C. Girit, M. Martin et al., Graphene plasmonics for tunable terahertz metamaterials. Nat. Nanotechnol. **6**, 630–634 (2011)
45. J.T. Liu, T.B. Wang, X.J. Li, N.H. Liu, Enhanced absorption of monolayer MoS_2 with resonant back reflector. J. Appl. Phys. **115**, 193511 (2014). https://doi.org/10.1063/1.4906398
46. Y.F. Liang, S.T. Huang, R. Soklaski, L. Yang, Quasiparticle band-edge energy and band offsets of monolayer of molybdenum and tungsten chalcogenides. Appl. Phys. Lett. **103**, 042106 (2013). https://doi.org/10.1063/1.4816517
47. C. Gong, H.J. Zhang, W.H. Wang, L.G. Colombo, R.M. Wallace et al., Band alignment of two-dimensional transition metal dichalcogenides: application in tunnel field effect transistors. Appl. Phys. Lett. **103**, 053513 (2013). https://doi.org/10.1063/1.4817409
48. M.M. Furchi, A. Pospischil, F. Libisch, J. Burgdörfer, T. Mueller, Photovoltaic effect in an electrically tunable van der Waals heterojunction. Nano Lett. **14**(8), 4785–4791 (2014). https://doi.org/10.1021/nl501962c
49. G.Y. Cao, A.X. Shang, C. Zhang, Y.P. Gong, S.J. Li et al., Optoelectronic investigation of monolayer MoS_2/WSe_2 vertical heterojunction photoconversion devices. Nano Energy **30**, 260–266 (2016). https://doi.org/10.1016/j.nanoen.2016.10.022